Arch. Metall. Mater., Vol. 61 (2016), No 2B, p. 1063–1067

DOI: 10.1515/amm-2016-0179

A. CYZA*#, Ł. CIENIEK*, A. KOPIA*

PEROVSKITE La1-xSrxFeO$_3$ THIN FILMS DEPOSITED BY LASER ABLATION PROCESS

The aim of the research was to investigate the influence of strontium on the structure of thin films La1-xSrxFeO$_3$ (x = 0; 0,1; 0,2). The LaFeO$_3$ and Sr-doped LaFeO3 films were produced by pulsed laser deposition (PLD) on Si (100) substrate using the Nd-YAG (λ = 266 nm) laser. SEM, AFM and XRD methods were used to characterize the structure and morphology of the thin films. X-Ray Diffraction analysis showed only the LaFeO$_3$ phase in the undoped thin film and the La0.9Sr0.1O$_3$ and La0.8Sr0.2O$_3$ phases in thin films doped by Sr. The mean crystallite size, calculated by Williamson-Hall method, was smaller (of the order of 18 nm) in films doped by Sr. SEM analysis showed small droplets in thin films doped by Sr. Highly developed surface layer was observed using the AFM microscope for thin films doped by Sr.

Keywords: Perovskite LaFeO$_3$, thin films, gas sensors, PLD

1. Introduction

Perovskite oxides with formula ABO_3 or A_2BO_4 are very important functional materials in various areas as: gas sensors [1,2], automotive exhaust catalysts [3,4], methane reformers that produce syngas [5,6], cathodes in solid oxide fuel cells (SOFCs) [7,8] or visible light photocatalysts [9,10]. The perovskite oxides (ABO_3) are used as gas sensor materials because of their thermal stability at higher temperature in different atmospheres. One of these materials is $LaFeO_3$. Perovskite $LaFeO_3$ has very good catalytic properties in the presence of gases like acetone (CH_3COCH_3), ethanol (C_2H_5OH), hydrogen sulphide (H_2S), hydrogen (H_2) [11], nitrogen dioxide NO_2 [12] and liquefied petroleum gas (LPG) [12]. Lee at al. [13] showed that Fe in $LaFeO_3$ perovskite structure is more active in catalytic reactions than La. In addition, Fe substituted by elements having the oxidation state of 2+ change the electronic structure of $LaFeO_3$ by the creation of free electrons and consequently influence on the catalytic properties. Thirumalairajan et al. [14] showed good selectivity and fast response-recovery time for NO_2 gas in thin films of $LaFeO_3$ doped by Co. Murade et al. [11] studied nanoparticles of La0.7Sr0.3O$_3$ and showed that they exhibit good sensing performances towards acetone gas with rapid response and high sensitivity at 548°K. Song et al. [15] found that Pb-doping could improve the sensitivity, selectivity and response time of $LaFeO_3$. Zangh et al. [16] studied the Ag-$LaFeO_3$ based sensor and found that the thin films showed higher response and better selectivity to formaldehyde. In all cases very important role play the surface of thin films and substituting of Fe or La by elements having the oxidation state of 2+. We can influence on the surface structure of thin films by modification of process parameters. Thin films of La1-xSrxO$_3$ are produced by MBE [17], PLD [2] and magnetron sputtering [13] methods. In our previous investigation [18] it were found optimal conditions for the deposition of nanocrystalline thin films of $LaCoO_3$ doped by Sr using laser ablation method. The study of the influence of Sr doping on the structure of $LaFeO_3$ thin films deposited by PLD is presented in this paper.

2. Experimental

2.1. Preparation of targets

The undoped $LaFeO_3$ targets were purchased from the Kurt J. Lesker Company. The powders of La1-xSrxO$_3$ (x = 0.1, 0.2) were prepared by mechanical alloying method. The powders La1-xSrxO$_3$ multiphase La_2O_3, La(OH)$_3$, La1-xSrxFeO$_3$ (x = 0, 0.1, 0.2) were milled in ball mill during t = 2, 4, 6, 10 hours using ZrO_2 balls. The powders were dried at temperature 973 K during 4 hours. Then, the targets were prepared by compacting the powders of La1-xSrxFeO$_3$ under a pressure of $p = 10^9$ Pa during 5 min then the pellets were sintered at T = 1623°K during 10 h.

2.2. Deposition of thin films

The La1-x SrxCoO$_3$ (x = 0, 0.1, 0.2) thin films were deposited on (100) oriented Si substrate using a laser ablation system equipped with the Nd-YAG (266 nm) laser and the chamber

* AGH-UNIVERSITY OF SCIENCE AND TECHNOLOGY, AL. A. MICKIEWICZA 30, 30-059 KRAKOW, POLAND

Corresponding author: annacyza@agh.edu.pl

Neocera. The parameters of the deposition system were as following: target-substrate distance $d = 70$ mm, the oxygen pressure in the deposition chamber $p = 5$ Pa and the laser beam incident angle on the target $\xi = 45°$. Substrates and target were parallel. The deposition conditions were: laser frequency $f = 10$ Hz, laser beam energy density on the target $\varepsilon = 2$ J/cm^2 and the substrate temperature 933°K.

2.3. Characterization of the target and thin films

The phase analyses of the target and thin films were performed by means of the X-ray diffraction method using PANanalytical EMPYREAN DY 1061 with Cu K_α radiation in Bragg-Brentano geometry and the grazing angle $\alpha = 1°$. PDF $^{4+}$ database of ICDD and CelRef software were used for phase identification and for calculation of the cell parameters, respectively. The surface morphology and chemical composition of the targets were analyzed using scanning electron microscope (SEM) FEI Inspect S50. The topography of the surface was investigated using atomic force microscope (AFM) Veeco Dimension® Icon™ SPM with NanoScope V.

3. Results and discussion

Phase compositions of the powders before mechanical alloying process were studied by X-Ray diffraction method in Bragg-Brentano geometry. Phases like $La(OH)_3$, La_2O_3, $La0.9Sr0.1O_3$ and $La0.8Sr0.2O_3$ were identified in powders (Fig. 1a,b). In order to obtain a homogeneous phase of powders, we proposed milling for 10 h and then annealing in temperature 973°K for 4 h. The XRD analysis of the powder before and after milling as well as after the annealing process are shown in Figure 1. The homogenous powders were obtain after 10 h milling (Fig. 1e,f).

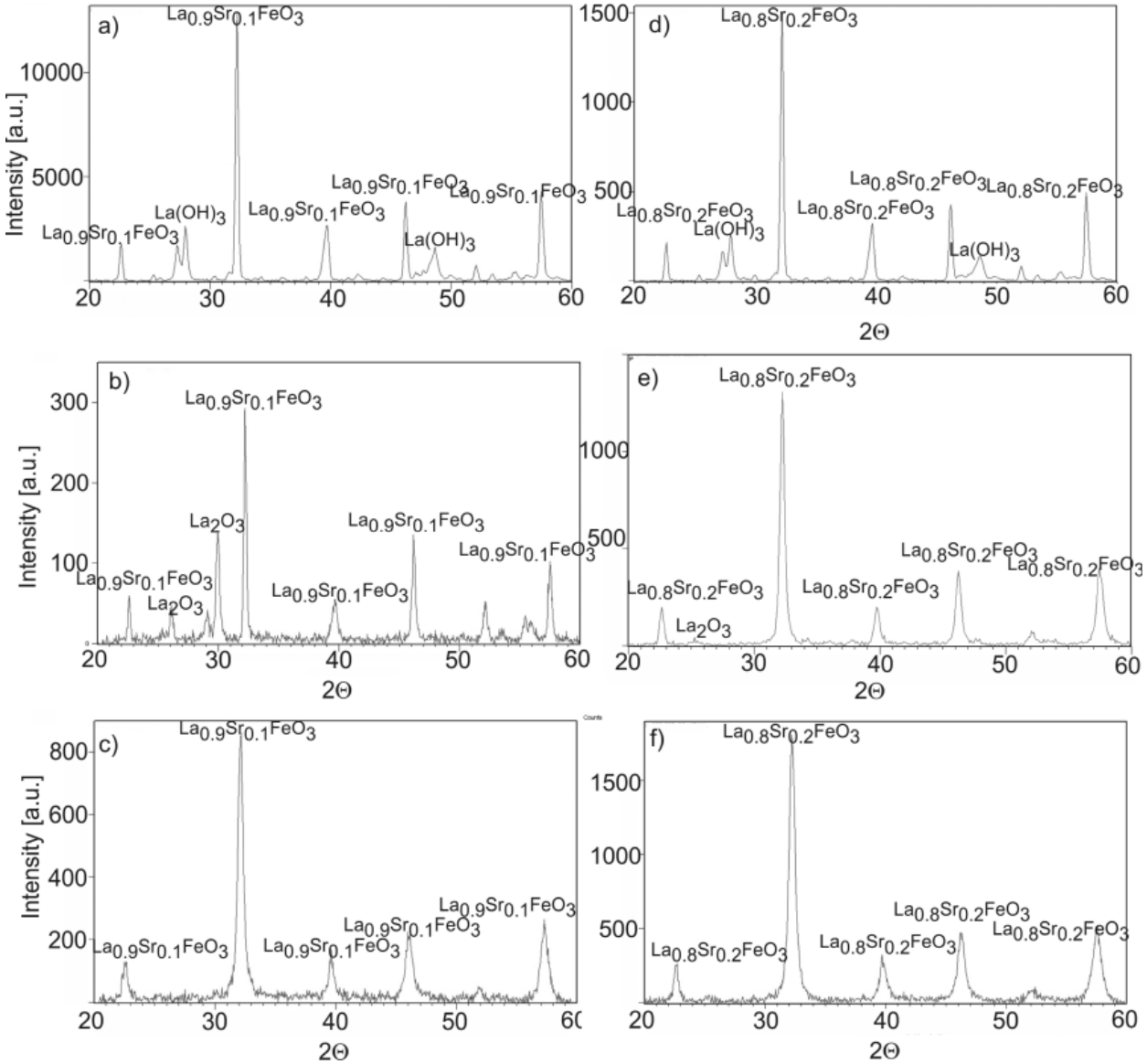

Fig. 1. XRD analysis of the powder a) deliver from producer $La_{0,9}Sr_{0,1}FeO_3$; b) deliver from producer $La_{0,8}Sr_{0,2}FeO_3$; c) after annealing $La_{0,9}Sr_{0,1}FeO_3$; d) after annealing $La_{0,8}Sr_{0,2}FeO_3$; e) after 10 h milling $La_{0,9}Sr_{0,1}FeO_3$; f) after 10 h milling $La_{0,8}Sr_{0,2}FeO_3$

The targets used for PLD process were formed from sintered powders of $La0.9Sr0.1O_3$ and $La0.8Sr0.2O_3$. The analysis of thin films was performed in Grazing geometry at the angle $\alpha = 1°$.The results are shown in Figure 2. The identification of phases was based on the JCPDS card number 04-008-0622, 04-007-6515, and 00-035-1480, for $LaFeO_3$, $La0.9Sr0.1O_3$, and $La0.8Sr0.2O_3$, respectively. The analysis of the diffraction patterns did not reveal the presence of other phases, such as La_2O_3, Fe_3O_4, and $SrCoO_3$.

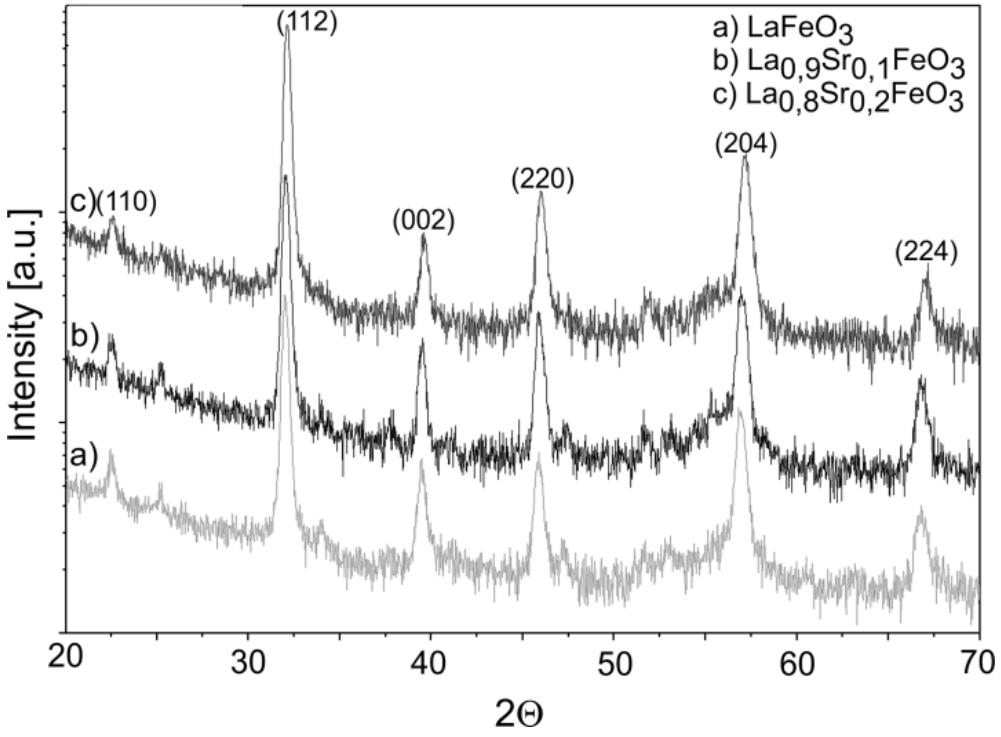

Fig. 2. XRD analysis of the thin films $La_{1-x}Sr_xFeO_3$

Based on received X-Ray patterns a depth of penetrating of X-ray was calculated (Eq. (1)) for $\alpha = 1°$ and $\alpha = 3°$. For $\alpha = 1°$ the calculated depth corresponds to d = 107 nm. On the diffraction pattern measured at $\alpha = 1°$ (Fig. 2c) it is visible an extention from diffraction line at about $2\theta = 52°$ that results from the support Si (100). Calculation by means of Eq. 1 suggests that mean thickness of the films studied is about 100 nm.

$$d = \frac{-ln\left(1 - G_x\right)}{\mu\left[\frac{1}{\sin\alpha} + \frac{1}{\sin\left(2\theta - \alpha\right)}\right]} \qquad (1)$$

d – effective depth of penetrating [μm], G_x – part of the total bent intensity x coming from the surface layer at depth (G_x = 0.8÷0.95), α – grazing angle of the radiation beam, θ – Bragg angle, μ – linear rate of the radiation absorption.

The average crystallite size in each layer was calculated. On the basis of the X-Ray results determined from the Williamson-Hall plot. The results are summarized in Table 1. For calculation we used only peaks (002), (112), (022), (004), (204). The crystallite size decreases with increasing Sr doping. The decreasing of the crystallite size may be due to the slowing of the crystal growth process [19]. Thus, doping of $LaFeO_3$ by Sr possibly affects the crystall growth rate, resulting in decreasing the mean grain size in these films.

TABLE 1

Structural parameters for Sr^{2+} doped $La_{1-x}Sr_xFeO_3$ (x = 0;0,1;0,2) perovskites

Compounds	$LaFeO_3$ (T = 30°C) [22]	X = 0	X = 0,1	X = 0,2
Crystal system space group Orthorhombic Pbnm-62 $\alpha = \beta = \gamma = 90°$				
Lattice parameters				
a = [nm]	0,5554	0,5566	0,5552	0,5522
b = [nm]	0,5556	0,5557	0,5545	0,5546
c = [nm]	0,7853	0,7856	0,7859	0,7837
Cell volume [nm^3]	242,3	242,9	241,96	240
Grain size D [nm]		36,8	18	21,1
Roughness R_a [nm]		2,27	5,57	7,97

At ambient conditions the lattice parameters of $LaFeO_3$ are: a = 0,5554 nm, b = 0,5556 nm and c = 0,7853 nm where $\alpha = \beta = \gamma = 90°$. In our $LaFeO_3$ thin film the lattice parameter is slightly higher that reported in the literature (Tab. 1). The increasing of lattice parameters in $LaFeO_3$ with increasing of the process temperature was observed by Selbach at al. [20]. Lattice parameters calculated for our $LaFeO_3$ film at temperature 933°K, the temperature of the support during PLD process, are in agreement with that refined by Selbach. This increasing lattice parameter and cell volume with temperature was explained by Selbach as transition of orthorhombic Pbnm phase to rhom-

bohedral R3c. The unit cell distortion subsequently increases gradually towards the transition to rhombohedral R3c at 1228°K. The linear thermal expansion coefficients between 500°K and 1200°K are α_a = 14.270±0.3×10^{-6}, α_b = 9.270±0.3×10^{-6}, and α_c = 12.470±0.3×10^{-6} [20]. Comparison of the diffraction patterns of the undoped and doped thin films (Fig. 2) showed the small moving of the diffraction lines (individual peaks) towards higher values of the 2 Θ. Calculated lattice parameters change with the increasing of Sr content. This is the effect of doping and changes of the oxidation state of Fe. The ionic radusi (8-coordinate) of La 3+ (0.13 nm) is slightly less than that of Sr 2+ (0.14 nm). To preserve the electro neutrality upon the substitution by atoms having the oxidation state of 2+, iron oxidation state increases from Fe 3+ towards Fe 4+. Taking into account the differences in the ionic radius of iron in oxidation states Fe 3+ (0,0645 nm) and Fe 4+ (0,0585 nm) we observed the decreasing of the cell volume [21,22]. Similar effects were observed in the system $LaFeO_3$ doped by Ca and Ti where the unit cell volumes decreased comparing to $LaFeO_3$ [21,22]. SEM images of La1-xSrxFeO_3 are show in (Fig. 3a-c). The $LaFeO_3$ thin film

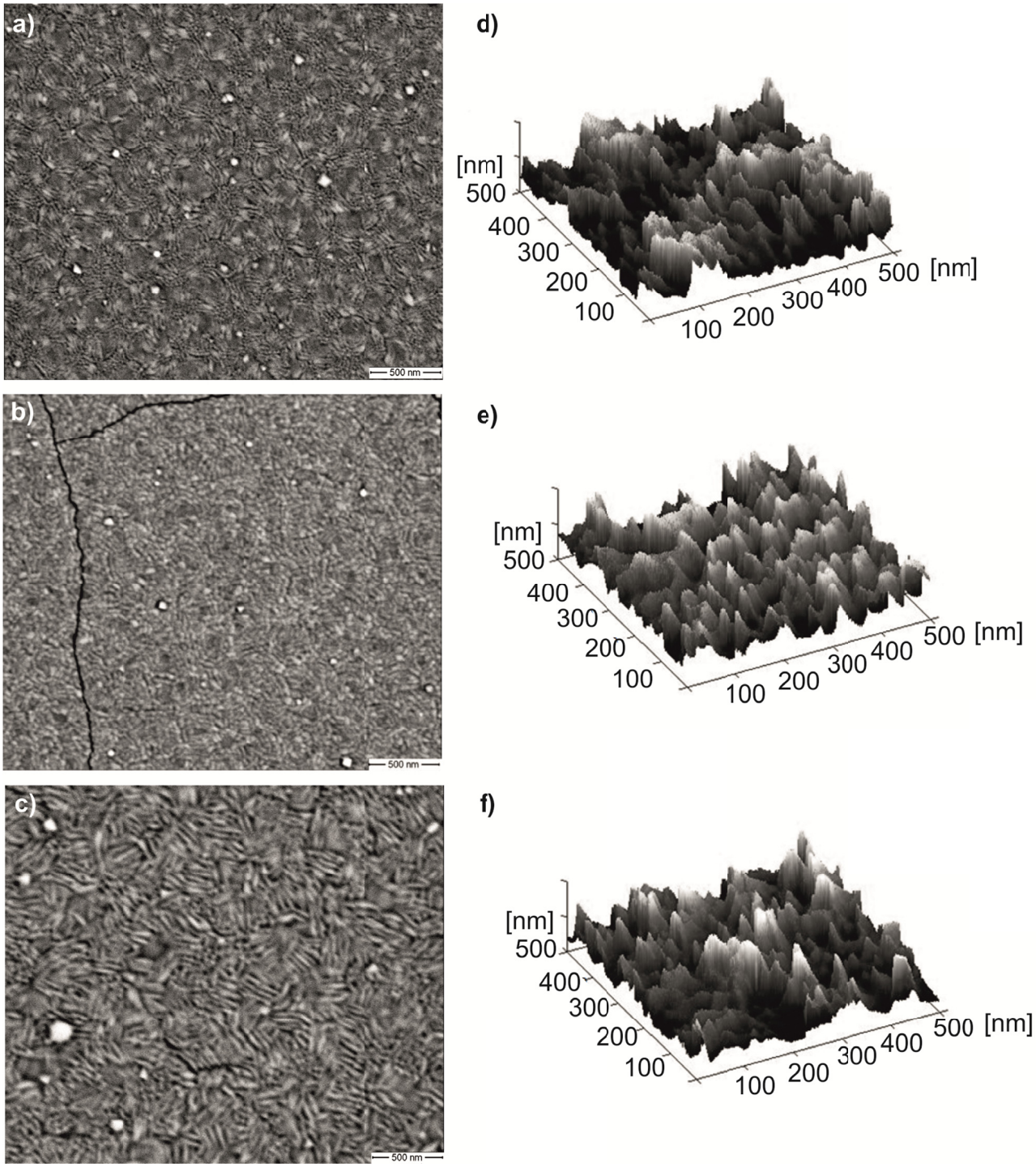

Fig. 3. Analysis by SEM: a) $LaFeO_3$; b) $La_{0,9}Sr_{0,1}FeO_3$; c) $La_{0,8}Sr_{0,2}FeO_3$ and AFM; d) $LaFeO_3$; e) $La_{0,9}Sr_{0,1}FeO_3$; f) $La_{0,8}Sr_{0,2}FeO_3$

is free from the droplets and cracks but the Sr-doped $LaFeO_3$ films have on the surface small droplets and the $La0.8Sr0.2O_3$ thin film is also cracked. The cracks are the consequence of to fast cooling process in this case. The structure of $La1\text{-}xSrxFeO_3$ thin films are nanocrystalline, the shape of the crystals does not change considerably upon Sr doping, what was observed in our previously investigation of $La1\text{-}xSrxCoO_3$ thin films [23].

Surface observations by AFM confirmed the results of the X-Ray analysis that the grain size of Sr-doped thin films was smaller than the grain size of the undoped $LaFeO_3$. Analysis by AFM was performed on 500×500 μm^2 area (Fig. 3d-f). On AFM scans we can observe refinement of the grain as a result of doping. The AFM results showed that the roughness parameter R_a (Table 1) is bigger in doped films.

4. Conclusions

The main objective of this research was to analyze the influence of strontium doping on the structure of $LaFeO_3$ films as potential material for gas sensor application and to deposit homogenous thin films of $La1\text{-}xSrxFeO_3$ using Pulsed Laser Deposition method. The study showed that the PLD process parameters were set correctly and it was possible to obtain nanocrystalline thin films of the assumed phase composition. The X-Ray diffraction patterns revealed only $LaFeO_3$ in undoped films and $La0.9Sr0.1O_3$ and $La0.8Sr0.2O_3$ phases in films a doped by Sr. Substitution of La by Sr caused the decrease of the grain size and the decreased cell volume witch can we explain by the blockade of crystalline growth. The decreasing of the grain size (calculated and observed by SEM) and increasing of the roughness parameter R_a determined by AFM might have positive impact on the sensitivity to gases due to the increase of the surface reactions efficiency.

Acknowledgements

This work was financially supported by the National Science Center through project number: UMO-2013/09/B/ST8/01681.

REFERENCES

[1] J.W. Fergus, Sensors and Actuators B. **123**, 1169 (2007).
[2] X. Liu, H. Ji, Y. Gu, M. Xu, Mat. Scien. and Eng. B **133**, 98 (2006).
[3] S. Furfori, N. Russo, D. Fino, G. Saracco, V. Specchia, Chem. Eng. Scien. **65**, 120 (2010).
[4] F. Patel, S. Patel, Proc. Engin. **51**, 324 (2013).
[5] H. Takamura, Membrane Reactors for Energy Applications and Basic Chemical Production, 519-54 (2015).
[6] K. Zhao, F. He, Z. Huang, A. Zheng, H. Li, Z. Zhao, Inter. J. of Hydr. Ener. **39**, 3243 (2014).
[7] O. Gwon, S. Yoo, J. Shin, G. Kim, Inter. J. of Hydr. Ener. **39**, 20806 (2014).
[8] X. Ding, W. Zhu, G. Hua, J. Li, Z. Wu, Electr. Acta **163**, 204 (2015).
[9] H. Li, S. Yin, Y. Wang, T. Sekino, S.W. Lee, T. Sato, J. of Cat. **297**, 65 (2013).
[10] S. Feraru, A.I. Borhan, P. Samoila, C. Mita, S. Cucu-Man, A.R. Iordan, M.N. Palamaru, J. Phot. and Phot. A, Chem. **307-308**, 1 (2015).
[11] P.A. Murade, V.S. Sangawar, G.N. Chaudhari, V.D. Kapse, A.U. Bajpeyee, Curr. Appl. Phys. **11**, 451 (2011).
[12] S. Thirumalairajan, K. Girija, V.R. Mastelaro, N. Ponpandian, Appl. Mater. Interf. **6**(16), 13917 (2014).
[13] Ch.W. Lee, R.K. Behera, S. Okamoto, R. Devanathan, E.D. Wachsman, S.R. Phillpot, S.B. Sinnott, J. Am. Ceram. Soc. **94**, 1931 (2011).
[14] S. Thirumalairajan, K. Girija, V. Ganesh, D. Mangalaraj, C. Viswanathan, N. Ponpandian, Cryst. Growth Des. **13**, 291 (2013).
[15] P. Song, H. Qin, L. Zhang, K. An, Zh. Lin, J. Hu, M. Jiang, Sens. and Actuat. B **104**, 312 (2005).
[16] Y.M. Zhang, Y.T. Lin, J.L. Chen, J. Zhang, Z.Q. Zhu, Q.J. Liu, Sens. and Actuat. B. Chemical **190**, 171 (2014).
[17] J.W. Seo, E.E. Fullerton, F. Nolting, A. Scholl, J. Fompeyrine, J.P. Locquet, J. Phys.: Condens. Matter **20**, 264014 (2008).
[18] M. Nistor, N.B. Mandache1, J. Perri`ere, J. Phys. D: Appl. Phys. **41**, 165205 (2008).
[19] R. Henda, G. Wilson, J.G. Munro, O. Alshekhli, A.M. McDonald, Thin Solid Films **520**, 1885 (2012).
[20] S.M. Selbach, J.R. Tolchard, A. Fossdal, T. Grande, Journal of Solid State Chemistry **196**, 249 (2012).
[21] S. Phokha, S. Hunpratup, S. Pinitsoontorn, B. Putasaeng, S. Rujirawat, S. Maensiri, Materials Research Bulletin **67**, 118 (2015).
[22] G. Pecchi, M.G. Jiliberto, A. Buljan, E.J. Delgado, Solid State Ionics **187,** 27 (2011).
[23] A. Kopia, Ł, Cieniek, K. Kowalski, J. Kusiński, Solid State Phenomena **231**, 19 (2015).